Design and Backdrivability Modeling of a Portable High Torque Robotic Knee Prosthesis With Intrinsic Compliance for Agile Activities

Junxi Zhu, Chunhai Jiao, Israel Dominguez, Shuangyue Yu, and Hao Su, *Member, IEEE*

***Abstract*—High-performance prostheses are crucial to enable versatile activities like walking, squatting, and running for lower extremity amputees. State-of-the-art prostheses are either not powerful enough to support demanding activities or have low compliance (low backdrivability) due to the use of high speed ratio transmission. Besides speed ratio, gearbox design is also crucial to the compliance of wearable robots, but its role is typically ignored in the design process. This article proposed an analytical backdrive torque model that accurately estimates the backdrive torque from both motor and transmission to inform the robot design. Following this model, this article also proposed methods for gear transmission design to improve compliance by reducing inertia of the knee prosthesis. We developed a knee prosthesis using a high torque actuator (built-in 9:1 planetary gear) with a customized 4:1 low-inertia planetary gearbox. Benchtop experiments show the backdrive torque model is accurate and proposed prosthesis can produce 200 Nm high peak torque (shield temperature $<$60 °C), high compliance (2.6 Nm backdrive torque), and high control accuracy (2.7/8.1/1.7 Nm RMS tracking errors for 1.25 m/s walking, 2 m/s running, and 0.25 Hz squatting, that are 5.4%/4.1%/1.4% of desired peak torques). Three able-bodied subject experiments showed our prosthesis could support agile and high-demanding activities.**

***Index Terms*—Backdrive torque modeling, high compliance, high torque actuator, powered prosthesis, wearable robots.**

Manuscript received January 20, 2022; revised March 28, 2022; accepted May 6, 2022. Recommended by Technical Editor Raffaella Carloni and Senior Editor Xiang Chen. This work was supported in part by the National Institutes of Health (NIH) R01 under Grant (1R01EB029765-01) and in part by the National Science Foundation Future of Work (2026622). *(Junxi Zhu and Chunhai Jiao are co-first authors.) (Corresponding author: Hao Su.)*

The authors are with the Laboratory of Biomechatronics and Intelligent Robotics, Department of Mechanical and Aerospace Engineering, North Carolina State University, Raleigh, NC 27695 USA (e-mail: jzhu35@ncsu.edu; cjiao000@citymail.cuny.edu; idoming@ncsu.edu; yushuangyue0221@gmail.com; hao.su796@ncsu.edu).

This work involved human subjects or animals in its research. Approval of all ethical and experimental procedures and protocols was granted by the Institutional Review Board at North Carolina State University (eIRB #24420), and performed in line with the NC State IRB Guidance.

This article has supplementary material provided by the authors and color versions of one or more figures available at https://doi.org/10.1109/TMECH.2022.3176255.

Digital Object Identifier 10.1109/TMECH.2022.3176255

I. Introduction

THERE are more than 6 00 000 people in the United States that have had lower limb amputations [1]. These subjects suffer great physical and mental pain due to low mobility, which prevents them from recovering and rejoining society. A common way to assist amputees in recovering basic mobility is using a prosthesis, either passive, semipowered, or powered. Passive prostheses are usually designed to be lightweight and low-cost but support walking tasks in a rigid and unnatural behavior. A semipowered prosthesis can achieve better performance to absorb impact and reduce the risk of falling for limited activities (e.g., walking) [2], [3].

To achieve assistance to agile activities, a fully powered prosthesis is required to produce higher torque than a semipowered design to satisfy the high energy requirements. But existing fully powered prostheses typically have to compromise compliance. This is because the high torque capability is usually achieved by the combination of high speed ratio transmission and low torque motor [4]–[6], while a large speed ratio causes high inertia and low compliance. Active compliance of a system is achieved through sensing and feedback control whereas intrinsic compliance is equivalent to the external torque needed to backdrive the system [7] and is affected by system properties such as friction and inertia. Low compliance is undesirable because residual limb and connection socket have to withstand considerable cyclic impacts from locomotion, which cause drastic discomfort to the amputee subjects and reduce the reliability of the prosthesis itself [8].

Prostheses that can generate high torque while remaining intrinsically compliant are crucial for agile activities. Though high active compliance is not achievable under high torque, intrinsic compliance is still maintained to ensure safety and comfort. Series elastic actuators (SEAs) [9] were developed to address the two requirements. By introducing an elastic component (typically a spring with a fixed stiffness) between the motor and end effector (Fig. 1), SEAs can enhance the compliance and absorb the external disturbance [5], [9], [10]. However, SEAs cannot adapt to different activities (such as walking, squatting, and running) because such activities impose a large range of stiffness requirements. In order to achieve the desired stiffness, variable stiffness actuators (VSAs) were introduced to overcome the shortcoming of SEAs. VSA paradigm can achieve finer control of the apparent stiffness by using two motors to modulate

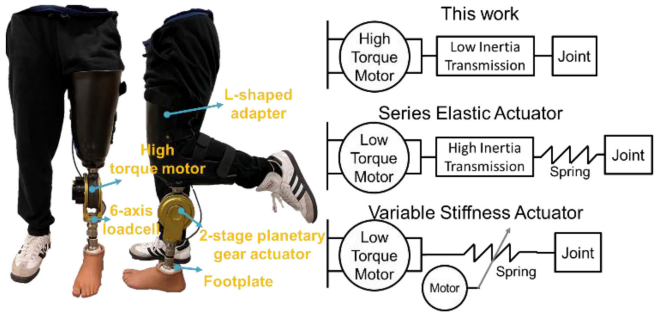

Fig. 1. Our prosthesis consists of a high torque motor and low inertia gear transmission, which can achieve high torque and high intrinsic compliance with a simple mechatronic design for portability. Our actuation paradigm can meet the multifaceted requirements of agile wearable robots, including high torque, high compliance, and simple design for portability.

both stiffness and equilibrium position [11]. However, both SEA and VSA add extra mass to the system due to extra elastic components, sensors, and/or motors. In addition, the use of elastic components improves compliance by sacrificing control bandwidth, which may not be suitable for activities that require fast response.

Attaining high torque and high intrinsic compliance while keeping a simple structure for portability of robotic prostheses requires innovative design of both motor and transmission. Our previous work [12], [13] employed a quasi-direct drive (QDD, transmission ratio $\leq 10:1$) actuation paradigm on a hip and knee exoskeleton that use high torque motor coupled with a low transmission ratio. This is a promising solution as it regulates the robot compliance *electronically* by controlling parameters in the motor control loop, whereas SEA and VSA achieve so by using mechanical structures (Fig. 1). *However, prior work only focused on the motor and did not consider the importance of the gear design to achieve high compliance of wearable robots.*

Backdrive torque is an important metric to assess the compliance performance of a robot. It is well-known that motor inertia and gear ratio are two keys to minimizing backdrive torque. However, transmission components such as gearboxes also have inertia and friction that are not negligible for a compliance model. Backdrive torque consists of acceleration-dependent terms and velocity-dependent terms, which are correlated with actuator inertia and friction, respectively. To improve the overall intrinsic compliance of an actuator while achieving higher torque capability, it is necessary to optimize the design of the transmission for low inertia and less friction. The selection and design of both motor and transmission need to be considered. Common ways to improve transmission compliance include using a small transmission ratio, reducing the number of rotary components, and improving transmission efficiency. There have been several work on improving the transmission efficiency by using a high-efficiency gearbox [14]–[16]. In this work, we designed a planetary gear transmission with low inertia to improve an actuator's overall compliance. We proposed a comprehensive actuation model that considers both motor and transmission to estimate the backdrive torque and is valuable to estimate the intrinsic compliance of the design before manufacturing, thus facilitating optimization in the early design phase.

TABLE I
DESIGN REQUIREMENTS OF KNEE PROSTHESIS

Parameters	1.25 m/s Walking	0.25 Hz Squatting	2.5 m/s Running	Our Design
Peak torque (Nm)	44	133	200	>200
Joint speed (rad/s)	4.3	2.4	8.1	8.1
Range of motion (deg)	10-60	0-130	15-90	0-130

The contributions of this article are as follows. First, this work proposed an analytical backdrive torque model that can accurately estimate the backdrive torque of a wearable robot. This model provided the principle to guide the design methods for highly compliant wearable robots and elucidated that highly compliant prostheses should consider both motor and gear transmission in the design. Second, this work proposed methods for the gear transmission design to improve compliance by reducing transmission inertia of a wearable robot. *To the best of authors' knowledge, this is the first work to take into consideration the effect of gear transmission through modeling and design methods to enhance the compliance of wearable robots.* Our prosthesis can generate a peak torque of 200 Nm with a backdrive torque of 2.6 Nm. The benchmark result shows our design has the highest torque capability with high output speed, indicating the proposed design has the potential to be used for agile activities (e.g., squatting and running) to further restore the mobility of lower extremity amputees.

II. KNEE BIOMECHANICS AND DESIGN REQUIREMENTS FOR AGILE ACTIVITIES

Walking, squatting, and running are all common activities in daily life. However, they impose significantly different torque and speed requirements. Using the biological references from the public dataset on able-bodied subjects, walking requires medium torque and medium speed, whereas squatting demands high torque and low speed. Running, on the other hand, demands both high torque and high speed. Based on the biological torque and speed profile for an 80 Kg subject [17]–[19], the knee joint needs to provide 44 Nm torque and 4.3 rad/s speed for walking at 1.25 m/s, 133 Nm torque, and 2.4 rad/s speed for full squatting at about 0.25 Hz, and 200 Nm torque and 8.1 rad/s speed for running at 2.5 m/s, as shown in Table I.

In addition, the prosthesis should also have high compliance to deliver more natural assistance to the user. It can also enable inertially driven swing motion, which is beneficial to the coordination with the thigh motion [3]. Our target is to design a compliant fully powered knee prosthesis that has smaller resistive torque than that of the biological knee joint, which is around 5 Nm calculated by the product of biological knee joint damping factor (about 1.1 $\mathrm{Nm}\cdot\mathrm{s/rad}$) and knee joint velocity (about 4.3 $\mathrm{rad/s}$) [20]. Finally, the prosthesis is required to be lightweight so that it is compatible with the sound limb and fits the natural movement of the residual limb. Based on one literature [21] studying the effect of prosthesis weight on

amputee subjects, our prosthesis should have less than 30% of the leg mass. Thus the prosthesis should weigh less than 3.8 Kg.

III. Mechatronics Design of High Torque and Compliant Knee Prosthesis

The main objective of the proposed portable powered knee prosthesis design is to achieve high output torque to enable agile tasks while still ensuring high compliance to reduce impact and save energy. This section detailed the modeling and design of our high torque and compliant knee prosthesis, including actuator paradigm, intrinsic compliance (represented by back-drive torque) modeling, and design of the low inertia planetary gearbox. The mechatronics design of the knee prosthesis is also presented.

A. Exterior Rotor High Torque Motor

The objective of motor design is to determine the actuation paradigm (high-torque motor with low gear ratio, or low-torque motor with high gear ratio) and which type of motor to use (exterior rotor or interior rotor). For the first objective, in a motor-gear transmission actuator system, actuator torque τ_{actuator} is proportional to motor torque τ_{motor} and transmission ratio N_{tran} as in (1). Therefore, high torque capability leverages a high torque motor, high transmission ratio, or their combination. On the other hand, the actuator compliance is related to the actuator reflected inertia as in (2), which is proportional to motor inertia and transmission ratio squared. High compliance leverages low actuator reflected inertia, which requires a low transmission ratio, low motor inertia, or their combination.

$$\tau_{\text{actuator}} = \tau_{\text{motor}} \times N_{\text{tran}} \tag{1}$$

$$I_{\text{reflected}} = I_{\text{motor}} \times N_{\text{tran}}^2. \tag{2}$$

It can be deducted from (1) and (2) that there is a tradeoff between high torque output and high compliance in terms of transmission ratio. In this section, we show in detail the underlying principles between the two and propose a method to satisfy the design requirements under these constraints. For a brushless direct current electric motor (BLDC), motor torque τ_{motor} is proportional to the motor length l and motor air gap radius squared r^2, and motor inertia I_{motor} is proportional to the motor stator length l and the motor air gap radius cubed r^3 as in (3) and (4) based on the motor scaling law in [22]. With the increase of motor torque τ_{motor}, motor inertia I_{motor}will also increase. Thus, higher torque capability of the actuator will certainly increase the actuator inertia. In the ideal condition, we assume the motor can be arbitrarily scaled to any size, the gearbox has no mass and friction, and the motor mass M_{motor} and actuator torque τ_{actuator} remain the same despite the size change. Motor stator mass typically makes up most of the motor overall mass. Assuming the same stator surface areal density, the stator mass (and thus the motor mass) is proportional to the motor stator length l and the motor air gap radius r as in (5) [22].

$$\tau_{\text{motor}} \propto lr^2 \tag{3}$$

$$I_{\text{motor}} \propto lr^3 \tag{4}$$

$$M_{\text{motor}} \propto lr. \tag{5}$$

To maintain the same actuator torque, the transmission ratio is inversely proportional to the motor torque. By further substituting (5) into this relationship, it shows the inverse proportionality between transmission ratio and air gap radius assuming that motor mass does not change with respect to size.

$$N_{\text{tran}} = \frac{\tau_{\text{actuator}}}{\tau_{\text{motor}}} \propto \frac{1}{lr^2} \propto \frac{1}{M_{\text{motor}} r} \propto \frac{1}{r}. \tag{6}$$

Combining (2), (4), and (6), the total actuator torque-inertia ratio is a constant and irrelevant to r as in (7). It indicates that large-radius high-torque pancake motors with a small transmission ratio and small-radius low torque cylindrical motors with a high transmission ratio should theoretically have the same reflected inertia.

$$\frac{\tau_{\text{actuator}}}{I_{\text{reflected}}} \propto \frac{lr^2 \times \frac{1}{r}}{lr^3 \times \left(\frac{1}{r}\right)^2} = 1. \tag{7}$$

However, torque-inertia ratio of the two paradigms is not a constant as in (7) once inertia and friction of the gearbox are considered. Previous studies [3], [5], [23] used a relatively large transmission ratio coupled with a low-torque motor. While these designs have relatively smaller mass and size, the large transmission ratio results in lower compliance, lower efficiency, and high frequency unpleasant audible noise [24]. Therefore, a large torque motor coupled with a small transmission ratio is preferred and would lead to improved performance [24]. The combination of a high torque motor with low ratio gear shows higher torque and compliance performance and was used in legged robots [25] and wearable robots [8], [12], [26].

For the second objective of motor design, to ensure that the actuator can produce large torque with a low transmission ratio, the motor itself should have high torque output capability to satisfy the demanding needs of agile activities. Previous studies modeled and validated two typical motor designs: interior rotor motor and exterior rotor motor [27], [28]. They showed that with a fixed motor axial length l and outer radius R, the exterior rotor motor has a higher output torque than the interior rotor motor. This is because the motor output torque is proportional to the product of the Lorentz force on the rotor and the air gap radius. Since the Lorentz force is also proportional to the motor stator area, then the motor output torque is proportional to the stator area and air gap radius. For an interior rotor motor, the stator area is proportional to $(R^2 - r^2)$, whereas for an exterior rotor motor, the stator area is proportional to r^2 [27]. Thus we obtain the relationship between motor output torque and air gap radius for both types of motors as shown in (8) and (9), where c is a common factor.

$$\tau_{\text{interior rotor}} = c\left(1 - \frac{r^2}{R^2}\right)\frac{r}{R} \tag{8}$$

$$\tau_{\text{exterior rotor}} = c\frac{r^3}{R^3}. \tag{9}$$

It can be observed that for an interior rotor motor, the output torque achieves its maximum when the rotor and stator of the interior rotor motor have the same area (i.e., $r = R/\sqrt{2}$). For an exterior rotor motor, however, the output torque grows

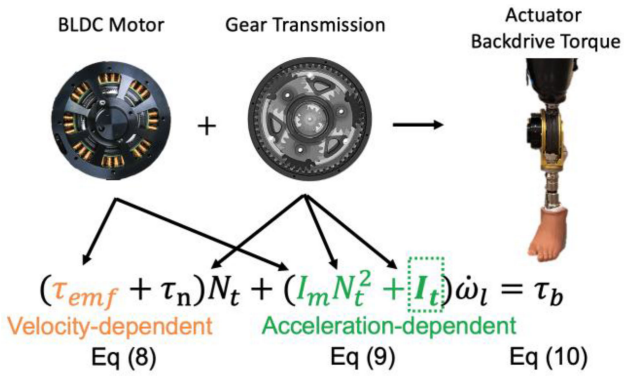

Fig. 2. Backdrive torque model for the actuator. τ_{emf} is the resistance moment caused by motor back electromotive force, and τ_{n} is the motor no-load torque. I_m and I_t are the inertia of the motor and transmission, respectively. N_t is the transmission ratio, $\dot{\omega}_l$ is the angular acceleration of the load, and τ_b is the overall backdrive torque of the actuator. The transmission inertia I_t (in the green box) is normally ignored in conventional robot design even though it should be considered.

monotonically as the stator area increases. Thus, an exterior rotor motor should be used to produce high torque.

In practice, the air gap radius r of an exterior rotor motor can be made as large as possible and close to R to maximize the torque output, as long as there is enough space for the rotor to produce the necessary magnetic field. Even though magnetic saturation is considered, exterior rotor motor can still produce higher torque than its internal rotor counterpart. In addition, the large hollow space at the center of the external rotor motor can accommodate a built-in small transmission ratio gearbox to step up the output torque and reduce the cogging effect. This makes the actuator compact which in turn makes the knee prosthesis less bulky. Therefore, the above-mentioned analysis informs us to use a new commercially available BLDC exterior rotor motor (T-motor AK10-9) with a high-torque low-speed characteristic, and it has a built-in 9:1 planetary gear transmission. It has a high torque constant of 0.16 Nm/A and can produce a nominal torque of 18 Nm and a peak torque of 48 Nm.

B. Modeling of Dynamic Backdrive Torque

Dynamic backdrive torque τ_b of an actuator, defined as the minimum torque to rotate the output at a particular speed and acceleration, is derived as in (10)–(12). It is a representation of the intrinsic robot compliance (compliance that does not rely on active control). In addition to transmission ratio and motor inertia, compliance is also affected by other design factors such as the inertia of rotary components and transmission efficiency. A transmission with low inertia is crucial to improving overall compliance performance. We proposed a backdrive torque model that considers both motor and transmission (Fig. 2).

$$\tau_{\text{emf}} = K_t \frac{\omega_m}{K_v R_{\text{motor}}}, \quad \tau_{\text{n}} = K_t I_0 \tag{10}$$

$$I_{\text{total}} = I_m N_t^2 + I_t, \quad I_t = \sum_j I_j N_j^2 \tag{11}$$

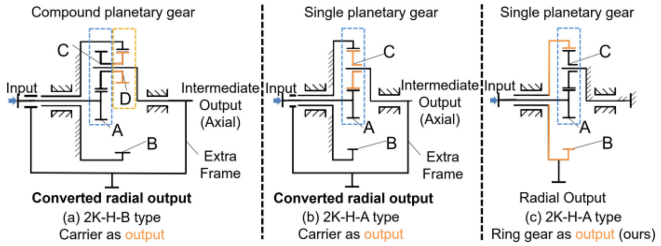

Fig. 3. (a) Compound planetary gear with planetary gear carrier as output [8]. (b) Single planetary gear with planetary gear carrier as output. (c) Single planetary gear with ring gear as output (ours). From (13)–(15), the selected single planetary gear with ring gear as output (c) has fewer rotary components (more compliant) compared with (a) and (b). A - sun gear, B - ring gear, C and D - planetary gears, X - planetary gear carrier.

TABLE II
PARAMETERS OF THE PLANETARY GEARSET

Gearset type	2K-H-A		
Transmission type	sun gear input, ring gear output		
Actual transmission ratio	3.93		
Gear modulus (mm)	2		
Center distance (mm)	35.5		
Teeth width (mm)	14		
Gears	A	B	C
Number of teeth	14	55	20
Addendum modification	0.55	0.3	0.57

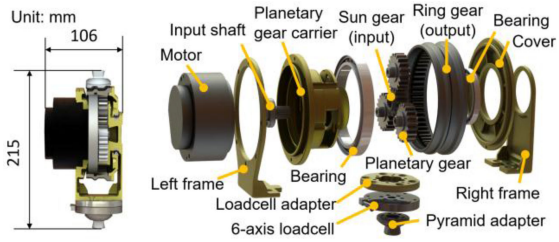

Fig. 4. Sectional and exploded view of our actuator design. By using sun gear as input and ring gear as output, we reduced the rotational inertia of the planetary gear carrier and revolution inertia of the planetary gears (15). The reduced overall inertia helps our actuator to achieve high intrinsic compliance.

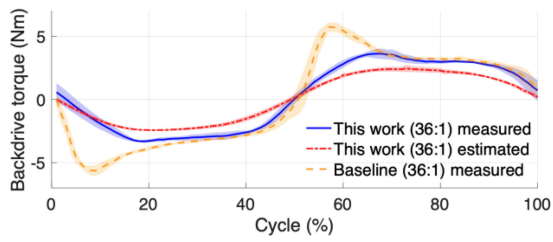

Fig. 5. Our actuator had 2.61 Nm RMS dynamic backdrive torque, which decreased 25% compared with a baseline actuator (3.57 Nm). Shaded areas show standard deviations. Our backdrive torque model using (10)–(12) can accurately estimate the actual backdrive torque, and thus is able to reflect the compliance of our actuator.

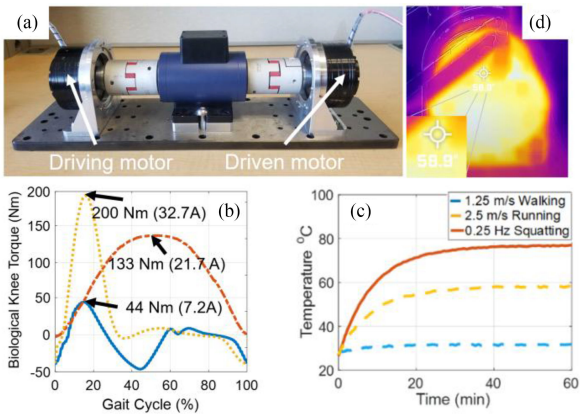

Fig. 6. Thermal test results show our designed knee prosthesis can continuously and safely provide desired assistance for agile activities. (a) Actuator dyno test platform. (b) Biological knee torque references for three activities used in the thermal test: walking (peak: 44 Nm, 7.2 A), running (peak: 200 Nm, 32.7 A), and squatting: (peak: 133 Nm, 21.7 A). (c) Motor winding temperature profiles for 60 m. (d) Observed maximum actuator shield temperature is 58.9 °C.

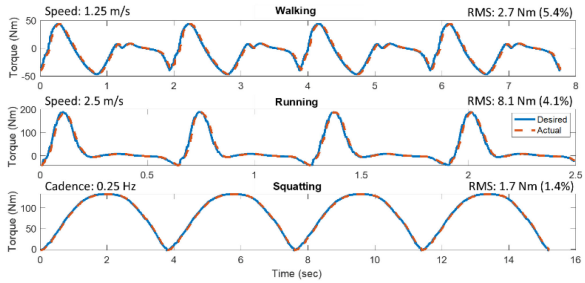

Fig. 7. Actuator torque tracking result for walking, running, and squatting. Our actuator achieves high tracking accuracy with an RMS error of 5.4%, 4.1%, and 1.4% of the torque magnitude, compared to about 7.8% error in [31].

$$\tau_b = \frac{(\tau_{\text{emf}} + \tau_n)\, N_t + I_{\text{total}}\dot{\omega}_l}{\eta}. \tag{12}$$

where η is the transmission efficiency, K_t and K_v are motor torque and velocity constant, R_{motor} is the winding resistance of the motor, and I_0 is the motor no-load current. The subscript j in I_{j} refers to any rotating component in the transmission, including a sun gear, planetary gear, carrier, bearings. N_t is the transmission ratio of the external second-stage gearbox, N_j is the speed ratio of the jth rotating component relative to the output.

C. Low-Inertia Compliant Gear Design

Once the motor is determined, the design of the external gearbox is the next important step to reaching high compliance. To reach 200 Nm peak torque, the prosthesis requires an external 4:1 gearbox besides the built-in 9:1 gear. For this gear ratio, a planetary gear transmission is an ideal option.

The first step of the compliant gearbox design is to determine the transmission type. In general, the transmission type can be divided into compound and single planetary gear according to the structural characteristics of the planetary gear. Compared with compound planetary gear that contains two stages, single planetary gear has a simpler structure and is suitable for low ratio transmission. In addition, in terms of the direction of the output, transmission type of the planetary gearset can be divided into axial output and radial output. For the axial output type, sun gear is usually active (input) and planetary gear carrier is passive with ring gear being fixed, where planetary gears rotate along their axis as well as revolve around the input shaft simultaneously. On the other hand, sun gear in the radial output type is usually active (input) and ring gear is passive with planetary gear carrier being fixed, where planetary gears rotate only along their axes. Although the advanced prosthesis design presented in [8] used the compound planetary gears with axial output transmission type as shown in Fig. 3(a), the single planetary gear structure with radial output type (ring gear as output) shown in Fig. 3(c) is more suitable for this case to maximize the compliance (low inertia). Compared with Fig. 3(a) and (b), this transmission type has the simplest structure and eliminates the need for extra components to convert the output direction, thus having a lower moment of inertia.

To show that our design in Fig. 3(c) results in the best compliance, moment of inertia of the three types in Fig. 3 were compared with each other. The simplified moment of inertia of the three different planetary gear transmission types, I_a, I_b and I_c, are derived in (13)–(15), respectively

$$I_a = \frac{1}{2} m_A r_A^2 + \frac{1}{2} m_C r_C^2 + \frac{1}{2} m_D r_D^2 + m_{\text{carrier}} r_{\text{carrier}}^2 + m_C (r_C + r_A)^2 + m_D (r_C + r_A)^2 + m_{\text{frame}} r_{\text{frame}}^2 \tag{13}$$

$$I_b = \frac{1}{2} m_A r_A^2 + \frac{1}{2} m_C r_C^2 + m_{\text{carrier}} r_{\text{carrier}}^2 + m_c r_c^2 + m_{\text{frame}} r_{\text{frame}}^2 \tag{14}$$

$$I_c = \frac{1}{2} m_A r_A^2 + \frac{1}{2} m_C r_C^2 + m_B r_B^2. \tag{15}$$

Assuming that three transmission types use the same sun gear, planetary gear, and ring gear, it can be deduced that our configuration in Fig. 3(c) (15) has the lowest moment of inertia because it uses the least components.

Once the transmission type is selected, the next step is to determine gear parameters (Table II). To maximize compliance, the design should make the structure of gearset as compact and lightweight as possible, meanwhile satisfying the boundary conditions such as overall transmission ratio and bending strength of the root of gear teeth. Therefore, our primary selection of the teeth number of sun gear z_A is 14, which is the minimum number without causing undercut during machining. Based on the overall transmission ratio requirement, assembly condition, and concentric condition (16)–(18), the teeth number of the ring gear z_B and the planetary gear z_C are determined as 55 and 20, where $N_t = 4$ is the target transmission ratio, $n_p = 3$ is the number of planetary gear, $[C]$ means C needs to be an integer, Δz_C is the reduction in the number of planetary gear teeth, which is 0.5, and is determined by the gear addendum modification such that z_C is an integer. The gear addendum modification is to enhance the contact strength and durability, which is commonly

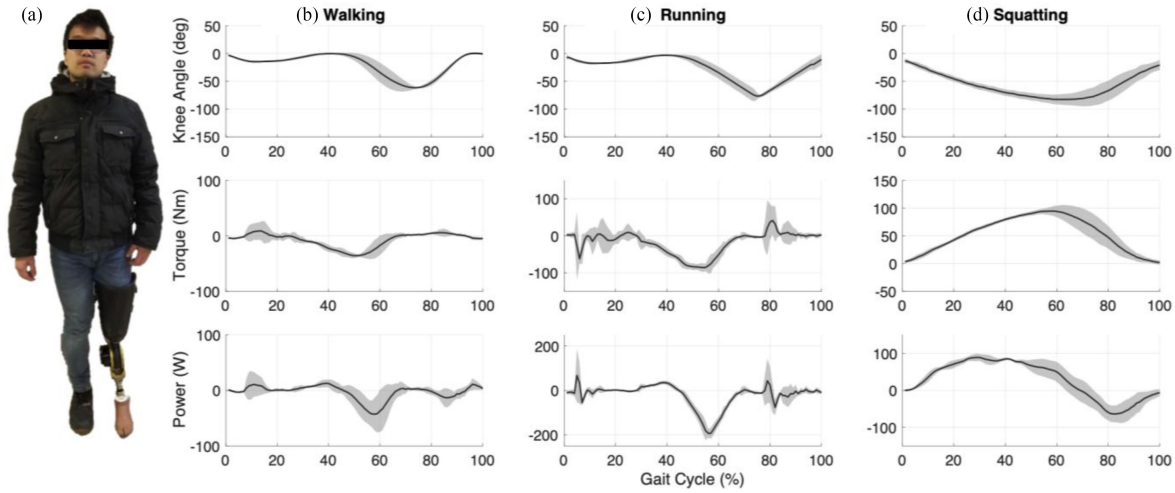

Fig. 8. (a) Able-bodied subject wearing the designed knee prosthesis. We show the averaged knee position, torque, and power profiles of the subject as well as biological values from the literature for (b) treadmill walking at 1.25 m/s, (c) running at 2 m/s, and (d) squatting at 0.25 Hz. Shaded areas show standard deviations. The results show that our prosthesis can support versatile high-demanding activities.

used for small gears.

$$z_B = z_A \times N_a \tag{16}$$

$$\frac{z_A + z_B}{n_p} = [C] \tag{17}$$

$$z_C = \frac{z_B - z_A}{2} - \Delta z_C. \tag{18}$$

According to (14), the actual transmission ratio $N_a = 55/14 = 3.93$, which has 1.75% error with the target transmission ratio $N_t = 4$ but falls within 5% error bound. Then, the gear modulus m was determined by (19), where $T_A = 54$ Nm, the coefficients $K_m = 12.1$, $K_A = 1.1$, $K_{F\Sigma} = 2$, $K_{FP} = 1.075$, $Y_{Fa1} = 2.25$, $\phi_d = 0.5$, $\sigma_{Flim} = 816$ MPa were obtained from [29]

$$m \geq K_m \sqrt[3]{\frac{T_A K_A K_{F\Sigma} K_{FP} Y_{Fa1}}{\phi_d z_a^2 \sigma_{Flim}}} = 1.85. \tag{19}$$

To make the gearbox as lightweight as possible, the gear modulus m was chosen to be 2. To ensure feasibility and reliability, bending strength verification was performed on the root of the gear teeth as in (20), where $d_1 = 28, b = 14, m = 2$ and the coefficients $K = 1.27$, $Y_{Sa1} = 1.76$, $Y_\varepsilon = 0.75$, $S_{Fmin} = 1.25, Y_N = 0.92, Y_{ST} = 2$ were obtained from [29]. It can be deduced that the actual bending stress σ_F is well below the maximum allowed bending stress $[\sigma_F]$.

$$\sigma_F = \frac{2000 K T_c}{d_1 b m} Y_{Fa1} Y_{Sa1} Y_\varepsilon = 519.6 \text{ MPa} < [\sigma_F]$$

$$= \frac{\sigma_{Flim} Y_{ST}}{S_{Fmin}} Y_N = 1201.1 \text{ MPa}. \tag{20}$$

Through the process earlier, the parameters of the compliant gear can finally be determined, as shown in Table II.

D. High Demanding Knee Prosthesis

The overall design of the knee prosthesis is shown in Fig. 1. It consists of an L-shaped adapter, a customized actuator, a six-axis loadcell, a pylon, and a footplate (Freedom Innovations, Australia). The control board, target PC, and the battery are tied around the waist of the subject. The weight of the knee actuator alone is 2.8 Kg, and the dimension is 215 mm (height) by 130 mm wide (medial-lateral) by 106 mm deep (anterior-posterior). The total weight of the knee prosthesis, including all the electronics and mechanical connection parts, is 3.3 Kg.

Particularly, with the radial output configuration in Fig. 3(c), the entire rotating components (ring gear and planetary gears) can be supported firmly through two large bearings at both ends of the actuator frame (Fig. 4). This simply supported setting makes load distribution more uniform, allowing for the reduced sectional size of the parts and thus reducing the weight. With more uniform loading and smaller deflection, better gear meshing is achieved, thus improving the transmission efficiency and durability.

E. Portable Electronics Design

In addition to portable mechanical design, the electronics also needs to be portable. A hierarchical control architecture was used in the controller design. The high-level controller gathers sensor data and detects human intention. The middle-level controller produces desired torque or position command, and the low-level controller implements these commands. A powerful Intel Atom x5 target computer was used as the high-level controller. The middle-level controller used an ARM Cortex-M4 microcontroller (Teensy 3.6) and communicated with the motor via CAN bus protocol. The onboard prosthesis sensors include two inertial measurement units (Alubi B2 IMU) on each thigh. A large-scale and lightweight 6-axis loadcell sensor (Sunrise Instruments, M3564F) measures the forces and torques applied to the knee

TABLE III
PERFORMANCE COMPARISON OF KNEE PROSTHESES

	Motor	Device Mass (Kg)	Maximum Transmission Ratio	Actuator Peak Torque (Nm)	Torque Density (Nm/Kg)	Actuator Speed (rad/s)	Actuator Peak Power[1] (kW)
MIT Knee [5]	Maxon EC-4 pole 30	2.7	143:1	120	44.4	12.1	1.45
Vanderbilt Leg [6]	Maxon EC-4 pole 30	5[2]	176:1	85	17.0	9.9	0.84
Utah AVT Knee [23]	Maxon EC-4 pole 22	1.6	375:1	125	78.1	4.7	0.59
OSL [10]	T-Motor U8	2.3	49.4:1	150	65.2	5.2	0.78
UMich Leg [8]	Robodrive ILM 85x26	6.0[2]	22:1	182	30.0	7.85	1.43
This work	**T-Motor AK10-9 KV60**	**3.3**	**36:1**	**200**	**58.18**	**8.12**	**1.62**

[1]The peak power is calculated from actuator peak torque and speed; [2]These devices include a powered ankle joint.

joint. The middle-level microcontroller is directly connected to the embedded electronics system of the motor using a CAN bus protocol.

IV. EXPERIMENTS

To demonstrate the performance of the knee prosthesis, we conducted both benchtop and human subject experiments. The benchtop experiments aimed to verify the accuracy of our model and design methods and evaluate the performance of the high torque and high compliance actuator, including backdrive torque, thermal property, and torque tracking. The human experiment shows the proposed knee prosthesis can provide high torque for agile activities.

A. Static Backdrive Torque Test (Robot Was Unpowered)

Static backdrive torque is the minimum torque required to drive the output while unpowered. We performed a static backdrive test to benchmark with state-of-the-art prosthesis. The knee actuator was fixed to the testbench, and we connected a rigid bar to the pyramid adapter on the ring gear. A force was applied to the end of the bar and the magnitude was gradually increased until the actuator just started to rotate. The reading from the loadcell was recorded and the static backdrive torque was taken as the maximum of the recorded moment. We repeated this experiment 6 times and the result was 2.63±0.06 Nm. In comparison, the static backdrive torque of the state-of-the-art high-torque prosthesis as in [8] was about 2.8 Nm, which had a smaller (22:1) transmission than our design.

B. Dynamic Backdrive Torque Test (Robot Was Unpowered)

We performed a dynamic backdrive torque test to evaluate the compliance of the knee actuator under the unpowered mode. We fixed the actuator onto the testbench and manually rotated the output ring gear between ±60° at a cadence of about 3 s and recorded the loadcell reading for 60 s. The cycles within the middle 40 s were averaged to obtain the mean backdrive torque profile and standard deviation.

To demonstrate the importance of transmission design, we compared our actuator with another similar baseline actuator in terms of dynamic backdrive torque. Both motors have similar rotor inertia and rated torque. The baseline actuator also has a 36:1 speed ratio but uses a planetary gearbox with planetary gear carrier as output [2K-H-B type, Fig. 3(b)]. It was tested in the same way as the actuator in this work for the dynamic backdrive torque. The result (Fig. 5) shows that our actuator had 2.61 Nm root-mean-square (RMS) dynamic backdrive torque, which is 25% less than the baseline actuator (3.57 Nm).

C. Thermal Property Test

A dynamometer test platform, as shown in Fig. 6(a), was set up to evaluate the thermal performance of the designed knee prosthesis. Two actuators were mounted as driving and driven actuators, respectively. The driving actuator was commanded in current control mode to provide a current that corresponds to the walking, squatting, and running biological torque profile as in Fig. 6(b) for our knee prosthesis. The driven actuator was commanded in position control mode (regulated at 0°) as a brake. We recorded the motor stator temperature as in Fig. 6(c) for a continuous 60 m for each activity, and the highest temperature stabled at 75.7 °C, much lower than 102.7 °C reported in [30] with a step reference. We also used a thermal meter (FLIR One, FLIR, Inc.) to monitor the actuator shield temperature. The peak actuator shield temperature for all three profiles stabilized at 58.9 °C as in Fig. 6(d) during squatting, which is below 60 °C threshold as specified by the ASTM C1055 standard for heated system surface conditions that produce contact burn injuries.

D. Torque Tracking Test for Prosthesis

Since our prosthesis is required to assist activities of vastly different torque requirements, we tested tracking performance during walking, running, and squatting assistance. The reference torque profile for these activities was taken from the public dataset for an 80 Kg subject [17]–[19]. The desired and measured torque are shown in Fig. 7 for all three activities. The actuator was able to track the desired trajectory with a RMS error of 2.7 Nm for walking, 8.1 Nm for running, and 1.7 Nm for squatting, corresponding to 5.4, 4.1, and 1.4% of the peak amplitude as shown in Fig. 8. The average acoustic level measured at the 1-meter distance was about 52 dB.

E. Knee Prosthesis for Walking, Running, and Squatting

Three able-bodied subjects (27.6 ±1.9 years, 70 ±1.6 Kg, and 173 ±2.5 cm) wore the prosthesis with an L-shape brace [Fig. 8(a)] and were tested for 1.25 m/s walking, 2 m/s running,

and 0.25 Hz deep squatting activities. The objective was to demonstrate that our knee prosthesis could sufficiently support high demanding versatile activities for different human subjects.

For the walking and running experiments, the subjects walked and ran on a treadmill at a constant speed for 2 m. The last 10 consecutive strides were used for analysis. For the squatting experiment, the subjects performed squatting at a cadence of 5 s 10 times. The last five consecutive squat cycles were chosen and used for analysis. Fig. 8(b)–(d) show the averaged knee position, torque and power trajectories, and standard deviations with respect to the gait cycle for walking, running, and squatting. The measured average peak torque (power) for walking, running, and squatting were 35.75 (42.77), 85.63 (193.02), and 105.16 (89.21) Nm (W), respectively.

V. Discussions and Conclusion

This article proposed an analytical backdrive torque model that can accurately estimate the compliance of wearable robot. This model provided the principle to guide the design methods for highly compliant wearable robots and elucidated that highly compliant prostheses should consider both motor and gear transmission in the design. This work also proposed methods for the transmission design to improve compliance by reducing transmission inertia of the knee prosthesis. Our result showed that the backdrive torque of our proposed knee prosthesis (2.6 Nm RMS) is 25% less than a baseline 36:1 actuator (3.5 Nm RMS). The proposed knee prosthesis can produce high peak torque (200 Nm) without overheating and with high control accuracy (2.7/8.1/1.7 Nm root mean square tracking errors for 1.25 m/s walking, 2 m/s running, and 0.25 Hz squatting, that are 5.4%/4.1%/1.4% of desired peak torques). Three able-bodied subject experiments showed our prosthesis could support agile and high-demanding activities such as 1.25 m/s walking, 2 m/s running, and 0.25 Hz squatting.

Table III benchmarked our design with the state-of-the-art knee prosthesis. Our design has the highest torque capability and output power, which has the potential to be used for agile activities to restore the mobility of lower extremity amputees. Compared with a high speed ratio based design ([5], [6], [23] in Table III), we eliminated the need for highly complex mechanical structures that result in extra weight or control complexities for the controller. Our design also avoids efficiency penalties due to high transmission ratio gearbox, considerable maintenance, remarkable acoustic noise, and large friction. Among the designs with low speed ratio transmission [8], [10], our prostheses have a larger torque and power output, which are necessary for supporting agile activities.

One limitation of the proposed knee prosthesis design is that we used a passive ankle joint, and thus toe tipping sometimes occurred that prevented the subject from walking or running naturally. A powered ankle would improve the coordination between the prosthesis and the residual limb and warrant a more biomimetic kinematic profile. Future work includes testing with amputees to assess the effect of the prosthesis. We believe our proposed design has the potential to restore the mobility of amputees and push forward the physics-informed design of personal mobility assistance devices.

References

[1] K. Ziegler-Graham, E. J. MacKenzie, P. L. Ephraim, T. G. Travison, and R. Brookmeyer, "Estimating the prevalence of limb loss in the United States: 2005 to 2050," *Arch. Phys. Med. Rehabil.*, vol. 89, no. 3, pp. 422–429, Mar. 2008.

[2] A. Kannenberg, B. Zacharias, and E. Pröbsting, "Benefits of microprocessor-controlled prosthetic knees to limited community ambulators: Systematic review," *J. Rehabil. Res. Develop.*, vol. 51, no. 10, pp. 1469–1496, 2014.

[3] J. T. Lee and M. Goldfarb, "Swing-assist for enhancing stair ambulation in a primarily-passive knee prosthesis," in *Proc. IEEE Int. Conf. Robot. Automat.*, 2020, pp. 740–746.

[4] T. Lenzi, M. Cempini, L. J. Hargrove, and T. A. Kuiken, "Design, development, and validation of a lightweight nonbackdrivable robotic ankle prosthesis," *IEEE/ASME Trans. Mechatronics*, vol. 24, no. 2, pp. 471–482, Apr. 2019.

[5] E. J. Rouse, L. M. Mooney, and H. M. Herr, "Clutchable series-elastic actuator: Implications for prosthetic knee design," *Int. J. Robot. Res.*, vol. 33, no. 13, pp. 1611–1625, Nov. 2014.

[6] B. E. Lawson, J. Mitchell, D. Truex, A. Shultz, E. Ledoux, and M. Goldfarb, "A robotic leg prosthesis: Design, control, and implementation," *IEEE Robot. Automat. Mag.*, vol. 21, no. 4, pp. 70–81, Dec. 2014.

[7] D. V. Gealy *et al.*, "Quasi-direct drive for low-cost compliant robotic manipulation," in *Proc. Int. Conf. Robot. Automat.*, 2019, pp. 437–443.

[8] T. Elery, S. Rezazadeh, C. Nesler, and R. D. Gregg, "Design and validation of a powered knee–ankle prosthesis with high-torque, low-impedance actuators," *IEEE Trans. Robot.*, vol. 36, no. 6, pp. 1649–1668, Dec. 2020.

[9] N. Paine, S. Oh, and L. Sentis, "Design and control considerations for high-performance series elastic actuators," *IEEE/ASME Trans. Mechatronics*, vol. 19, no. 3, pp. 1080–1091, Jun. 2014.

[10] A. F. Azocar, L. M. Mooney, J.-F. Duval, A. M. Simon, L. J. Hargrove, and E. J. Rouse, "Design and clinical implementation of an open-source bionic leg," *Nature Biomed. Eng.*, vol. 4, no. 10, pp. 941–953, Oct. 2020.

[11] D. J. Braun, V. Chalvet, T.-H. Chong, S. S. Apte, and N. Hogan, "Variable stiffness spring actuators for low-energy-cost human augmentation," *IEEE Trans. Robot.*, vol. 35, no. 6, pp. 1435–1449, Dec. 2019.

[12] S. Yu *et al.*, "Quasi-direct drive actuation for a lightweight hip exoskeleton with high backdrivability and high bandwidth," *IEEE/ASME Trans. Mechatronics*, vol. 25, no. 4, pp. 1794–1802, Aug. 2020.

[13] J. Wang *et al.*, "Comfort-centered design of a lightweight and backdrivable knee exoskeleton," *IEEE Robot. Automat. Lett.*, vol. 3, no. 4, pp. 4265–4272, Oct. 2018.

[14] H. Matsuki, K. Nagano, and Y. Fujimoto, "Bilateral drive gear—A highly backdrivable reduction gearbox for robotic actuators," *IEEE/ASME Trans. Mechatronics*, vol. 24, no. 6, pp. 2661–2673, Dec. 2019.

[15] S. Crispel *et al.*, "A novel wolfrom-based gearbox for robotic actuators," *IEEE/ASME Trans. Mechatronics*, vol. 26, no. 4, pp. 1980–1988, Aug. 2021.

[16] T. Ishida and A. Takanishi, "A robot actuator development with high backdrivability," in *Proc. IEEE Conf. Robot., Automat. Mechatronics*, 2006, pp. 1–6.

[17] R. K. Fukuchi, C. A. Fukuchi, and M. Duarte, "A public dataset of running biomechanics and the effects of running speed on lower extremity kinematics and kinetics," *PeerJ*, vol. 5, May 2017, Art. no. e3298.

[18] C. A. Fukuchi, R. K. Fukuchi, and M. Duarte, "A public dataset of overground and treadmill walking kinematics and kinetics in healthy individuals," *PeerJ*, vol. 6, Apr. 2018, Art. no. e4640.

[19] S. Yu *et al.*, "Design and control of a high-torque and highly backdrivable hybrid soft exoskeleton for knee injury prevention during squatting," *IEEE Robot. Automat. Lett.*, vol. 4, no. 4, pp. 4579–4586, Oct. 2019.

[20] J. T. Lee, H. L. Bartlett, and M. Goldfarb, "Design of a semipowered stance-control swing-assist transfemoral prosthesis," *IEEE/ASME Trans. Mechatronics*, vol. 25, no. 1, pp. 175–184, Feb. 2020.

[21] J. M. Czerniecki, A. Gitter, and K. Weaver, "Effect of alterations in prosthetic shank mass on the metabolic costs of ambulation in above-knee amputees," *Amer. J. Phys. Med. Rehabil.*, vol. 73, no. 5, pp. 348–352, Sep. 1994.

[22] S. Seok, A. Wang, D. Otten, and S. Kim, "Actuator design for high force proprioceptive control in fast legged locomotion," in *Proc. IEEE/RSJ Int. Conf. Intell. Robots Syst.*, 2012, pp. 1970–1975.

[23] M. Tran, L. Gabert, M. Cempini, and T. Lenzi, "A lightweight, efficient fully powered knee prosthesis with actively variable transmission," *IEEE Robot. Automat. Lett.*, vol. 4, no. 2, pp. 1186–1193, Apr. 2019.

[24] M. E. Carney, T. Shu, R. Stolyarov, J.-F. Duval, and H. M. Herr, "Design and preliminary results of a reaction force series elastic actuator for bionic knee and ankle prostheses," *IEEE Trans. Med. Robot. Bionics*, vol. 3, no. 3, pp. 542–553, Aug. 2021.

[25] S. Kim and P. M. Wensing, "Design of dynamic legged robots," *FNT Robot.*, vol. 5, no. 2, pp. 117–190, 2017.

[26] D. Lee, B. McLain, I. Kang, and A. Young, "Biomechanical comparison of assistance strategies using a bilateral robotic knee exoskeleton," *IEEE Trans. Biomed. Eng.*, vol. 68, no. 9, pp. 2870–2879, Sep. 2021.

[27] T. Reichert, T. Nussbaumer, and J. W. Kolar, "Torque scaling laws for interior and exterior rotor permanent magnet machines," in *Proc. IEEE Int. Magn. Conf.*, 2009, pp. 1–4.

[28] J. W. Sensinger, S. D. Clark, and J. F. Schorsch, "Exterior vs. interior rotors in robotic brushless motors," in *Proc. IEEE Int. Conf. Robot. Automat.*, 2011, pp. 2764–2770.

[29] R. G. Budynas and J. K. Nisbett, *Shigley's Mechanical Engineering Design*, 9th ed. New York, NY, USA: McGraw-Hill, 2011.

[30] U. H. Lee, C.-W. Pan, and E. J. Rouse, "Empirical characterization of a high-performance exterior-rotor type brushless DC motor and drive," in *Proc. IEEE/RSJ Int. Conf. Intell. Robots Syst.*, 2019, pp. 8018–8025.

[31] T. Lenzi, M. Cempini, L. Hargrove, and T. Kuiken, "Design, development, and testing of a lightweight hybrid robotic knee prosthesis," *Int. J. Robot. Res.*, vol. 37, no. 8, pp. 953–976, Jul. 2018.